MNE 19 (2023) 100187

Contents lists available at ScienceDirect

Micro and Nano Engineering

journal homepage: www.sciencedirect.com/journal/micro-and-nano-engineering

Modelling and nanofabrication of chiral dielectric metasurfaces

Luca Fagiani [a], Marco Gandolfi [b,c,d], Luca Carletti [b,c,d], Costantino de Angelis [b,c,d], Johann Osmond [e], Monica Bollani [f,*]

[a] Department of Physics, Politecnico di Milano, Piazza Leonardo Da Vinci 32, 20133 Milano, Italy
[b] Department of Information Engineering, University of Brescia, Via Branze 38, 25123 Brescia, Italy
[c] INO-CNR, Via Branze 45, Brescia, 25123, Italy
[d] CNIT, Viale G.P. Uberi 181/A, 43124 Parma, Italy
[e] ICFO (Institut de Ciencies Fotoniques), The Barcelona Institute of Science and Technology, 08860 Castelldefels, (Barcelona), Spain
[f] CNR - IFN, LNESS Laboratory, Via Anzani 42, 22100 Como, Italy

ARTICLE INFO

Keywords:
Chiral metasurface
Circular dichroism
Dielectric metasurface
Quality factor
EBL
Third-harmonic generation

ABSTRACT

Polarization control through all-dielectric metasurfaces holds great potential in different fields, such as telecommunications, biochemistry and holography. Asymmetric chiral metasurfaces supporting quasi-bound states in the continuum may prove very useful for controlling and manipulating the polarization state of light. A crucial quantity for characterizing the optical chirality is the circular dichroism (CD). In this work we analyse how the CD and quality factor of the optical mode can be strongly influenced by a nanofabrication error. Modelling the nanofabrication uncertainties on the gaps of the chiral metasurface, the imperfections of the etchings process or the modification of the asymmetry factor, we found that the proper engineering of the gap between the nanostructures of the unit cell is the most important parameter to achieve a high-quality factor and enhanced optical dichroism. An optimization of the nanofabrication processes, such as dose factor, dwell time and plasma etching demonstrates that, for a writing field of 100 μm^2, it is possible to obtain morphologically precise chiral metasurfaces, with fabrication uncertainties lower than those that would limit Q factor and chirality property.

1. Introduction

Planar optics carry fundamental and technological interests for miniaturizing and simplifying optical systems [1,2]. In particular, metasurfaces – realized by covering a surface with sub-wavelength structures – allow the manipulation of the incident light with a high degree of control [3]. Another advantage of metasurfaces is the limited weight and volume, thus enabling novel functionalities and improving the performances offered by bulk optical components or lenses [4]. Optical metasurfaces are often described as the two-dimensional versions of bulk metamaterials [5]. They typically consist of a single or a few sub-wavelength thickness layers of designed nanoscale building blocks arranged in an ordered geometry over a flat surface. These ordered nanostructures possess unique capabilities to fully control light within a subwavelength layer [6,7] including wavelength- and polarization-selective control of complex diffraction [8–10]. A relevant application of metasurfaces is the control and the manipulation of the polarization state of a light beam. Precisely, chiral metasurfaces may respond in a much different way upon illumination with a circular polarization with respect to the other one. These differences may be quantified by introducing the concept of circular dichroism (CD) [11]. An intriguing phenomenon is nonlinear chiral circular dichroism, which consists in a nonlinear optical response that depends on the handedness of the incident light. To observe such phenomena, given the small thickness of metasurfaces, optical resonances with a high quality-factor are necessary. Symmetric metasurfaces can support symmetry-protected bound states in the continuum (BIC), i.e. optical modes with an infinite quality (Q) factor. These modes are dark because the symmetry forbids the coupling to an external excitation and the incident radiation. However, by slightly breaking the symmetry, the BIC evolves into quasi-BIC (q-BIC) with a finite (but high) Q-factor. In other words, the external radiation starts interacting with the mode and an intriguing alteration of the optical response may set in. The stronger is the asymmetry, the lower is the Q-factor [12–14]. If the broken symmetry structure is pumped at the q-BIC wavelength, the stored electromagnetic energy inside it becomes very high, thus considerably enhancing the nonlinear optical processes. These ideas were merged in ref. [15], where a silicon metasurface is engineered to have a BIC mode in the telecom wavelength. By

* Corresponding author.
E-mail address: monica.bollani@ifn.cnr.it (M. Bollani).

https://doi.org/10.1016/j.mne.2023.100187
Received 15 December 2022; Received in revised form 6 March 2023; Accepted 5 April 2023
Available online 6 April 2023

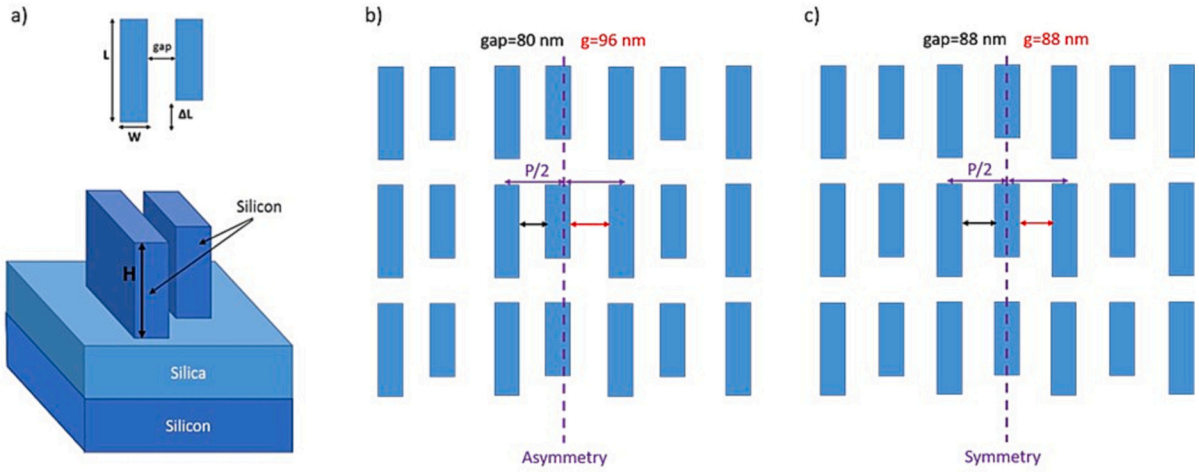

Fig. 1. a) In the bottom panel, a sketch of the unit cell composing the chiral metasurface and a top view of the unit cell is reported in top panel. b) Top view of the fabricated asymmetric metasurface, yielding the maximum value of THCD. c) Sketch of the metasurface when the gap increases to 88 nm, endowed with an additional symmetry plane with respect to the fabricated metasurface.

breaking the symmetry, the structure became at the same time chiral - paving the way to an important CD - and very efficient in the third-harmonic generation if pumped at the q-BIC wavelength. These two facts allow also to detect a high circular dichroism in the third-harmonic signal (THCD). However, the fabrication of such a metasurface is not straight-forward and some technical problems may arise. Indeed, one of the key questions for the metasurface community is how to fabricate these optical platforms both on a laboratory scale and in high volume production. Designing and fabricating optical metasurfaces requires to carefully assess the level of precision that needs to be reached to warrant the realization of the desired optical functionality with good efficiency [16–18]. The discrepancies between the optical simulated response and measured performances of metasurfaces are commonly ascribed to nanofabrication imperfections, due to the different nanolithography and dry etching problems.

The aim of this work is to describe the processes of the fabrication of a broken-symmetry metasurface endowed with a q-BIC. The admissible experimental tolerances in order not to compromise the q-BIC functioning of the dielectric metasurfaces are modelled. Specifically, the optical performances of the non-ideal metasurface are simulated as functions of the geometrical parameters affected by the fabrication errors This work is beneficial for the design and realization of planar optical metasurfaces offering a great potential for biomedical sensing, environmental and healthcare monitoring, or quantum computing applications.

2. Materials and methods

The choice of the silicon as material for the chiral metasurface in this work is due for its high compatibility with CMOS technology, low-cost fabrication, and high refractive index. The metasurface platforms based on high refractive-index dielectric materials such as silicon, indeed, are promising for sever fields, since they exhibit low losses with respect to their metal counterparts [19,20]. For this activity, the chiral metasurface consists of a matrix of asymmetric Si cuboids on silica substrate as schematized in Fig. 1a and b, where the definition of its unit cell composed by the two asymmetric cuboids with the same height, but different side dimensions, is reported. One cuboid has side length L, whereas the second block is shortened by ΔL with respect to the first. When ΔL=0 the metasurface is symmetric and a BIC is present. On the other hand, if ΔL increases, the in-plane symmetry is broken, and the BIC evolves into q-BIC. The broken symmetry can be quantified with the asymmetry parameter $\alpha = \Delta L/L$. The patterned nanoantenna elements are built on the top wafer acting as a device layer with a thickness of 220 nm. The buried silicon oxide layer (2 μm) is an excellent electric insulating layer, and it also forms an effective etch-stop in device manufacturing [21,22]. In general, it can also act as a sacrificial layer when manufacturing more complex devices such as released MEMS structures. The handle (001) Si wafer is supporting the optical platform. The optimized parameters are calculated by considering a height (H) of 220 nm for all the blocks in the chiral metasurface.

2.1. Finite elements simulations

In this section we introduce finite elements simulations, in order to find the geometrical parameters maximizing the THCD in correspondence of the q-BIC mode. To this purpose, we calculate the optical modes of the metasurfaces with COMSOL Multiphysics, Wave Optics Module. The optical eigenmodes of the structure have been calculated following the approach described in Ref. [15], and from the obtained complex eigenfrequencies $\tilde{\nu}$ we derive the modal Q-factor as:

$$Q = \frac{1}{2}\frac{Re(\tilde{\nu})}{Im(\tilde{\nu})}.$$

where $\tilde{\nu}$ is the frequency of the eigenmode. We calculate the average intensity enhancement within the two blocks $<I_{en,\,RH}>$ when the pump is right-handed circularly polarized (RCP), defined as:

$$< I_{en,RH} >= \frac{1}{V}\int_V \frac{I(\boldsymbol{r})}{I_0} dV,$$

where V is the volume of the two blocks in the unit cell, $I(\boldsymbol{r})$ is the spatially dependent light intensity and I_0 is the intensity of the RCP incident pump. Analogously, we also compute the intensity enhancement $<I_{en,\,LH}>$ when the pump is left-handed circularly polarized (LCP).

As shown in ref. [15], a maximum of the intensity enhancement corresponds to a peak of the third harmonic conversion efficiency. Therefore, the THCD can be calculated as the intensity enhancement CD, i.e.:

$$THCD = \frac{\left|\langle I_{en,LH} > - < I_{en,RH} > \right|}{< I_{en,LH} > + < I_{en,RH} >}.$$

The ideal metasurface is obtained by tuning the geometrical parameters periodicity, width, length, gap, and asymmetry parameter of the structure as long as a configuration with a q-BIC with a high THCD is observed. The best solution has been found for a periodicity (P) of 850 nm, a width (W) of 337 nm, a length (L) of 550 nm, a gap of 80 nm, and asymmetry parameter (α) of 0.32. The chiral behaviour is guaranteed by

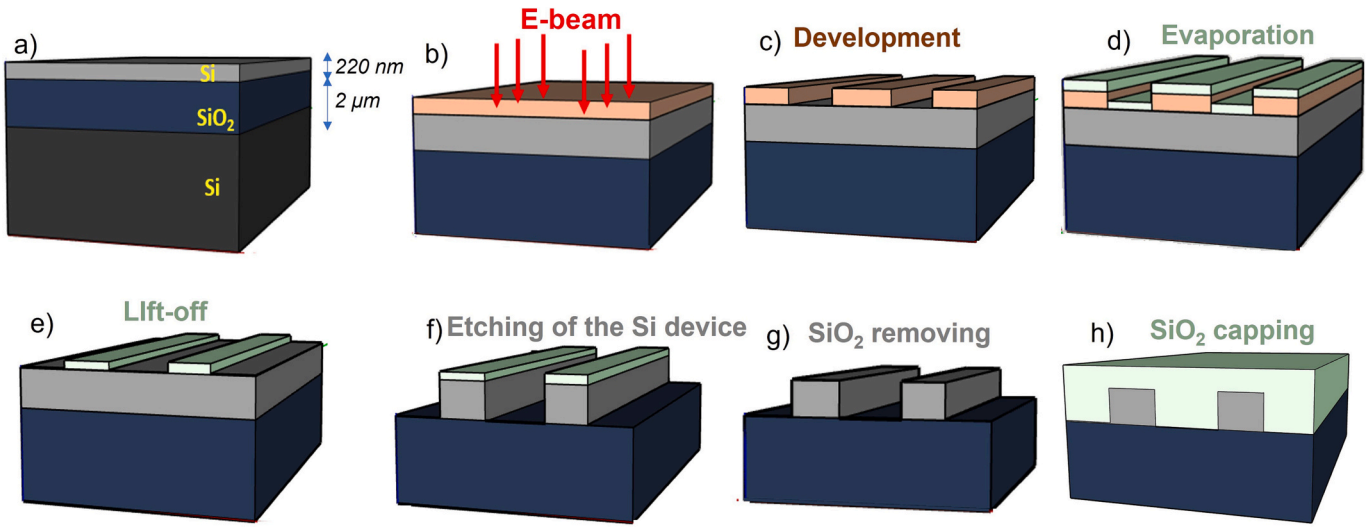

Fig. 2. Representation of the nanofabrication standard process used to realize all chiral metasurfaces. (a) SOI wafer sketch; (b) exposure of the spin-coated sample and (c) development of the exposed area; Deposition of ~45 nm of SiO_2 used as hard mask (d) and lift-off of the SiO_2 mask (e), the Si layer is etched by ICP-RIE; (g) removal of the hard mask and (h) final deposition of a thick layer of SiO_2 to have all the metasurfaces embedded in the silica. For the sake of visualization, the domains are drawn not in scale.

the asymmetry of the structure: in fact, with this choice of parameters the distance between two adjacent cuboids of adjacent unit cells (referred as g) is 96 nm that is different with respect to the gap dimension (80 nm). The presence of this asymmetry justifies the chiral activity of the device that instead wouldn't be observable for a gap dimension of 88 nm. In the latter case g equals the gap, thus introducing a symmetry plan (Fig. 1c).

We point out that if the metasurface is in air (and no silica superstrate is added), the optimal parameters configuration yields a q-BIC with high THCD at a light wavelength around 1420 nm. However, we are interested in moving the q-BIC around the telecom wavelength (1.55 μm) for technological applications. To this purpose, we need to embed all the metasurface into silica and this can be done by adding a silica capping.

2.2. Fabrication

The samples in this study are prepared on a 1.5 × 1.5 cm^2 silicon on insulator (SOI) wafer (Fig. 2a). Firstly, as a standard nanofabrication procedure common to all SOI samples, a cleaning in hot acetone solution at 28 °C for 5 min and an isopropanol (IPA) rinse is carried out. Then a single layer of positive resist (Poly(methyl methacrylate, PMMA)), is spin-coated on SOI surfaces baked at 160 °C for 5 min to ensure that the resist thickness is approximately 120 nm (Fig. 2b). The samples are then exposed by electron beam lithography (EBL). The patterned areas are for all chiral metasurfaces 100 × 100 μm^2. After the EBL exposure is completed, the sample are immersed in a developer solution in proportion to the 3:1 in volume of isopropanol and methylisobutyl ketone for 75 s to remove the PMMA exposed part. A pure IPA solution is used for 60 s to stop the development (Fig. 2c). After that, 45 nm of SiO_2 are deposited on the samples (Fig. 2d) through e-beam evaporation. The samples are then left into pure acetone solution for at least 3 h to allow the dissolution of the remaining resist, preserving the patterned zone (Fig. 2e) by SiO_2 film. The patterned silica is used as hard mask for the dry etching process (Fig. 2 f). After the dry etching, the hard mask is clearly observable from scanning electron microscope (SEM) characterization, showing that the original thickness (H) 220 is preserved. Finally, the remaining hard mask is removed with a quick passage (20 s) in a 5% in vol HF solution (Fig. 2g). After that, it is performed a mechanical polishing of the back of the sample with a diamond suspension of particle (curvature radius 1 μm). The last step of fabrication consists of another evaporation of ~350 nm of SiO_2 as a capping layer (Fig. 2h). The metasurface with the ideal parameters owns a quasi-BIC at the

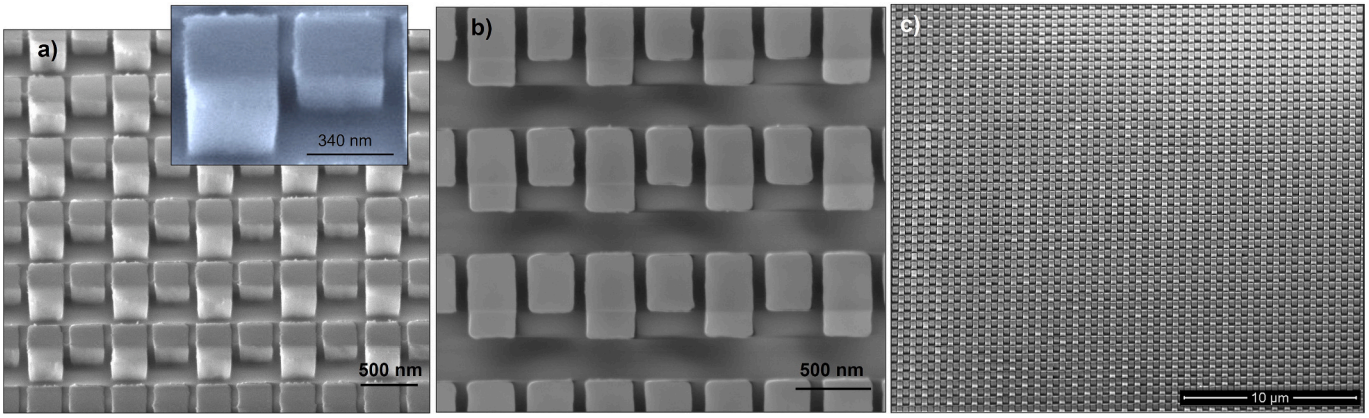

Fig. 3. SEM images of chiral metasurfaces taken before the last SiO_2 deposition. The nanostrucutres (a) in the tilted view and (b) in the planar view are not deteriorated significantly after the dry etching process. Panel c) shows a tilted SEM image of a large patterned area, confirming the homogeneity of the EBL and RIE porcesses working with write fields fileds of 100 μm^2.

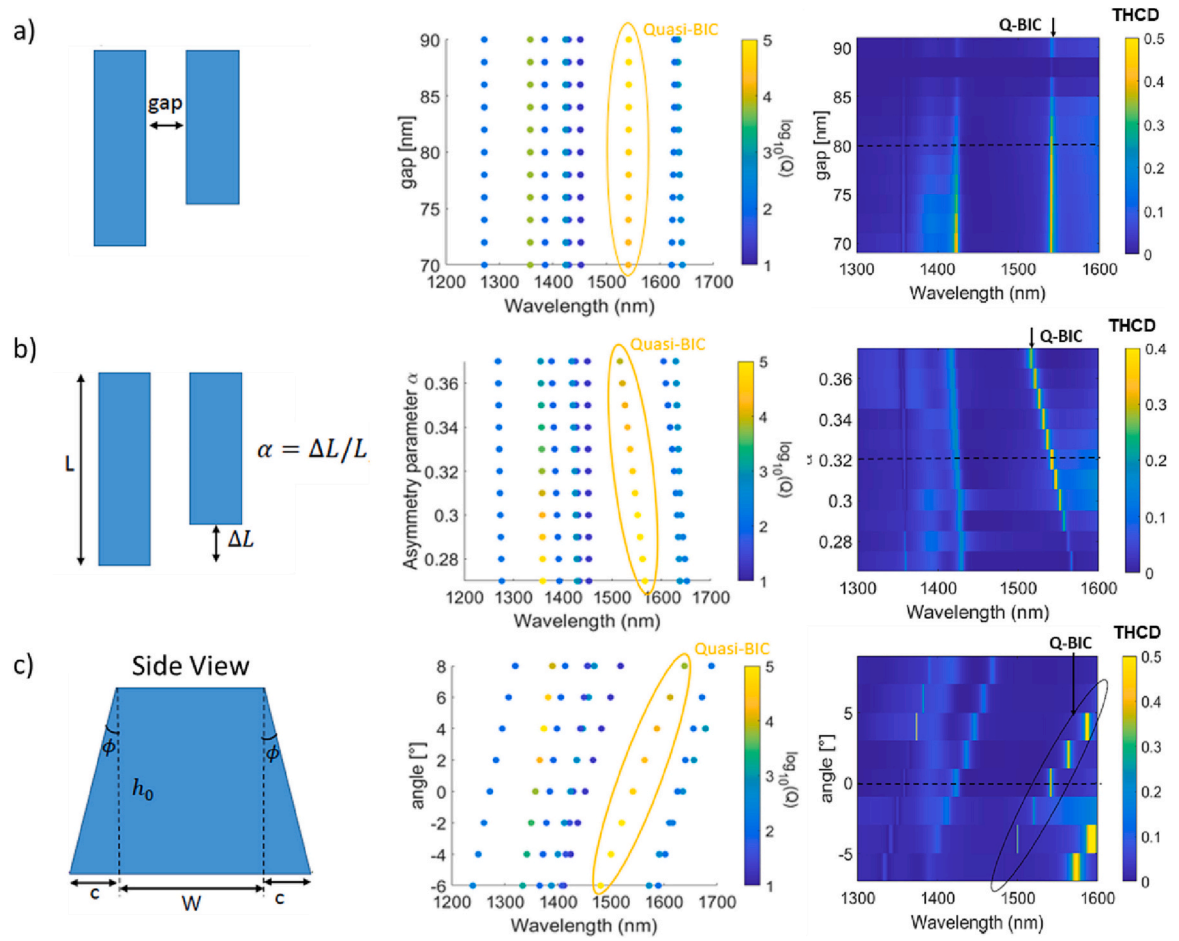

Fig. 4. Left panels: Sketch of the geometrical parameters that are investigated with finite elements method (top view of the unit cell in panels a and b, side view in panel c). Central panels: wavelength (horizontal axis) of the metasurface modes as a function of the inquired geometrical parameter (vertical axis). The Q-factor of the modes is superimposed on the markers as a colour. The q-BIC are highlighted by a yellow circle. Right panels: THCD (colour scale) as function of the light wavelength of the incident light (horizontal axis) and of the inquired geometrical parameter (vertical axis). The q-BIC mode is highlighted with black circles or arrows. The dashed horizontal lines indicate the parameter of the ideal geometry. The inquired geometrical parameter is the gap (a), the asymmetry parameter α (b) or the angle of the vertical walls φ (c). (For interpretation of the references to colour in this figure legend, the reader is referred to the web version of this article.)

telecom wavelength with a high Q-factor (~10^5) and with an important THCD. The final configuration of the metasurface reports the Si blocks completely embedded in silica, a necessary condition to have the q-BIC at third telecom wavelength.

3. Results and discussion

3.1. Nano fabrication optimization of the metasurface

A SEM modified EBL system from Raith with an acceleration voltage of 30 kV is used, testing PMMA as positive resist. The final optimized dose used for all chiral metasurfaces exposure is ~320 μC/cm^2. These are the optimized conditions to avoid overdose problems during the exposure and to obtain a gap of about 80 nm (± 5 nm). A similar uncertainty is also found for the other geometrical parameters (L and W), corresponding to the minimum resolution available for our SEM. All exposed samples are then etched. In order to guarantee a minimum roughness of the walls and achieve the verticality of the etching process, a process with inductively coupled plasma reactive ion etching (ICP-RIE) is preferred over an etching with only the RIE process. The optimized etching parameters for the chiral metasurfaces are therefore a mixture plasma of C_4F_8 (60 sccm) and SF_6 (45 sccm) for 1 min with a radio frequency generation power of 15 W and ICP power of 800 W. From cross view SEM characterizations, we see that the maximum φ angle, calculated between the lateral sides and the direction normal to the substrate, is less than 1°, while the uncertainty on the ΔL and the gap, measured in planar view is lower than the 5 nm. SEM images of the optimized chiral metasurfaces are finally reported in Fig. 3.

In Fig. 3a a tilt SEM image of the optimized chiral metasurface is reported. In the zoom it is possible to appreciate the low roughness of the etching process and a minimum under etching, lower than 1°, calculated at the base of the structure. A planar view image is indeed shown in Fig. 3b, from which the measurements of the widths and lengths of the single unit cells, the gap between the structures and the periodicity are measured. A gap of 80 nm is obtained between the longest and the shortest cuboids in the unit cell, while the gap between one cuboid and the closest one in the proximal unit cell is 96 nm, confirming a periodicity of 850 nm along x and y directions. On overview of the patterned area is represented in Fig. 3c. The optimization of the EBL and ICP-RIE parameters are obtained using an EBL write field of 100 μm^2. Finally, the reproducibility of the optimized process is validated by processing three different samples batches.

3.2. Effects of the fabrication incertitude on the optical results

Since q-BICs may be sensitive with respect to imperfections in the fabrication, a detailed analysis on the effects introduced by introducing small tolerances in the geometrical parameters have been performed with COMSOL Multiphysics. In particular, the analyses consider three key challenging aspects of the fabricated structures: the gap between the

two cuboids (Fig. 4a), the value of the asymmetry parameter α (Fig. 4b), and finally, the inclination of the lateral walls of the cuboids induced by the dry etching (Fig. 4c).

On the left panels of Fig. 4 the investigated geometries are described, whereas in the middle panel we report the wavelength of the metasurfaces modes (horizontal axis) as function of the investigated geometrical parameters (vertical axis). The colour superimposed on the markers indicate the Q-factor of each mode. Finally, on the right panel we report THCD as a function of the pump beam wavelength (horizontal axis) and of the investigated geometrical parameter (vertical axis). Considering the gap variation, it can be observed that by increasing or decreasing its dimension of 10 nm the Q factor and the spectral position of the q-BICs remains basically constant (Fig. 4a). As for the THCD, the situation is different: for values above 85 nm as gap, the CD contribute is drastically suppressed. Indeed, for a gap dimension of 88 nm the system acquires symmetry thus losing its chiral properties, as schematized in Fig. 1c.

In Fig. 4b the asymmetry parameter α is studied. Small changes strongly perturb the q-BICs, in fact the transition from perfect BICs to q-BICs and their detection is ruled by the asymmetry parameter. A decrement of the 25% of α in proximity of its optimal value (0.32) leads to an enhancement of its Q factor together with a red shift of the mode of ≈ 30 nm. This phenomenon is also associated with almost a suppression of the THCD, whose value drops from 0.5 to 0.1. The line associated to THCD maxima follows exactly the spectral position of the q-BICs in the central panel, confirming the direct correlation between these two parameters.

Finally, to mimic a real etch profile we consider not-straight vertical walls. To simulate this situation, we consider the angle φ between the lateral sides and the direction normal to the substrate. The ideal metasurface has $\varphi = 0$ and the angle is varied to simulate an under etching and over etching effect that can occur during RIE process (Fig. 4c). Both THCD and Q are highly dependent on this parameter. The q-BICs shows a red shift of more than 100 nm tuning φ from -5° to 5, while the Q-factor shows a small reduction. On the other hand, the nonlinear CD shows that for negative angles, including $\varphi = -2^\circ$, the effect is suppressed, while for positive angle (5 °C) the signal is almost doubled respect to the standard 0° configuration.

As a conclusion, from COMSOL simulation it emerges that the most sensible parameter is the gap between two cuboids: a small variation from 80 nm can potentially suppress the circular dichroism. However, considering that the maximum experimental uncertainty on the measurement of the gap between the nanostructures is below 5 nm, as well as the under-etching angle is at most 1°, we can conclude that the optimized EBL and RIE parameters here reported prove the ability to realize chiral metasurfaces without compromising the CD and Q factor. Linear and non-linear optical characterizations, which are not the scope of this work, will also confirm the optical quality of these metasurfaces.

4. Conclusions

In this paper, asymmetric chiral metasurfaces, endowed with q-BIC states at telecom wavelength, are studied. An optimized nanofabrication is carried out, showing that by a 30 kV EBL system it is possible to obtain chiral metasurfaces on a write field 100 μm^2 with minimal variations between the repetition of the single unit cell. By means of finite elements method, we computed how the most common nanofabrication errors affect the optical readout. In particular, the effects of the experimental defects on the metasurfaces have been calculated in terms of quality factor and third-harmonic circular dichroism. The nanofabrication errors obtained after the optimization of the nanolithography and etching processes are lower than the simulated tolerances. These results pave the way to design optical metasurfaces suitable for a plethora of applications that span from environmental and healthcare monitoring, biological sensing, or quantum computing.

Declaration of Competing Interest

The authors declare that they have no known competing financial interests or personal relationships that could have appeared to influence the work reported in this paper.

Data availability

Data will be made available on request.

Acknowledgements

We acknowledge funding from the Russian Science Foundation grant n° 22-12-00204 and the Ministero dell'Istruzione, dell'Università e della Ricerca (grant n° 2017MP7F8F). M. G. acknowledges financial support by European Union “FESR o FSE, PON Ricerca e Innovazione 2014-2020 - DM 1062/2021”.

References

[1] C.W. Qiu, T. Zhang, G. Hu, Y. Kivshar, Quo vadis, metasurfaces? Nano Lett. 21 (13) (2021) 5461–5474.
[2] D. Rocco, M. Gandolfi, A. Tognazzi, O. Pashina, G. Zograf, K. Frizyuk, C. De Angelis, Opto-thermally controlled beam steering in nonlinear all-dielectric metastructures, Opt. Express 29 (23) (2021) 37128–37139.
[3] M. Khorasaninejad, F. Capasso, Metalenses: versatile multifunctional photonic components, Science 358 (6367) (2017) eaam8100.
[4] J. Yang, S. Gurung, S. Bej, P. Ni, H.W.H. Lee, Active optical metasurfaces: comprehensive review on physics, mechanisms, and prospective applications, Rep. Prog. Phys. 85 (3) (2022), 036101.
[5] A. Vaskin, R. Kolkowski, A.F. Koenderink, I. Staude, Light-emitting metasurfaces, Nanophotonics 8 (7) (2019) 1151–1198, 8.
[6] X. Luo, Subwavelength optical engineering with metasurface waves, Adv. Opt. Mater. 6 (7) (2018) 1701201.
[7] A.S. Solntsev, G.S. Agarwal, Y.S. Kivshar, Metasurfaces for quantum photonics, Nat. Photonics 15 (5) (2021) 327–336.
[8] Y.F. Yu, A.Y. Zhu, R. Paniagua-Domínguez, Y.H. Fu, B. Luk'yanchuk, A. I. Kuznetsov, High-transmission dielectric metasurface with 2π phase control at visible wavelengths, Laser Photonics Rev. 9 (4) (2015) 412–418.
[9] K.I. Okhlopkov, A. Zilli, A. Tognazzi, D. Rocco, L. Fagiani, E. Mafakheri, A. A. Fedyanin, Tailoring third-harmonic diffraction efficiency by hybrid modes in high-Q metasurfaces, Nano Lett. 21 (24) (2021) 10438–10445.
[10] A. Tognazzi, K.I. Okhlopkov, A. Zilli, D. Rocco, L. Fagiani, E. Mafakheri, C. De Angelis, Third-harmonic light polarization control in magnetically resonant silicon metasurfaces, Opt. Express 29 (8) (2021) 11605–11612.
[11] M.L. Solomon, J. Hu, M. Lawrence, A. García-Etxarri, J.A. Dionne, Enantiospecific optical enhancement of chiral sensing and separation with dielectric metasurfaces, ACS Photon. 6 (1) (2018) 43–49.
[12] Z. Liu, Y. Xu, Y. Lin, J. Xiang, T. Feng, Q. Cao, J. Liu, High-Q quasibound states in the continuum for nonlinear metasurfaces, Phys. Rev. Lett. 123 (25) (2019), 253901.
[13] P. Hu, J. Wang, Q. Jiang, J. Wang, L. Shi, D. Han, J. Zi, Global phase diagram of bound states in the continuum, Optica 9 (12) (2022) 1353–1361.
[14] K. Koshelev, S. Lepeshov, M. Liu, A. Bogdanov, Y. Kivshar, Asymmetric metasurfaces with high-Q resonances governed by bound states in the continuum, Phys. Rev. Lett. 121 (19) (2018), 193903.
[15] M. Gandolfi, A. Tognazzi, D. Rocco, C. De Angelis, L. Carletti, Near-unity third-harmonic circular dichroism driven by a quasibound state in the continuum in asymmetric silicon metasurfaces, Phys. Rev. A 104 (2) (2021), 023524.
[16] V.C. Su, C.H. Chu, G. Sun, D.P. Tsai, Advances in optical metasurfaces: fabrication and applications, Opt. Express 26 (10) (2018) 13148–13182.
[17] L. Fagiani, A. Zilli, A. Tognazzi, E. Mafakheri, K. Okhlopkov, Silicon metasurfaces with tunable electromagnetic resonances for nonlinear optical conversion, Il nuovo cimento C 44 (4–5) (2021) 1–4.
[18] A. Patoux, G. Agez, C. Girard, V. Paillard, P.R. Wiecha, A. Lecestre, A. Arbouet, Challenges in nanofabrication for efficient optical metasurfaces, Sci. Rep. 11 (1) (2021) 1–12.
[19] M.R. Shcherbakov, P.P. Vabishchevich, A.S. Shorokhov, K.E. Chong, D.Y. Choi, I. Staude, Y.S. Kivshar, Ultrafast all-optical switching with magnetic resonances in nonlinear dielectric nanostructures, Nano Lett. 15 (10) (2015) 6985–6990.
[20] P. Genevet, F. Capasso, F. Aieta, M. Khorasaninejad, R. Devlin, Recent advances in planar optics: from plasmonic to dielectric metasurfaces, Optica 4 (1) (2017) 139–152.
[21] M. Bollani, M. Salvalaglio, A. Benali, M. Bouabdellaoui, M. Naffouti, M. Lodari, M. Abbarchi, Templated dewetting of single-crystal sub-millimeter-long nanowires and on-chip silicon circuits, Nat. Commun. 10 (1) (2019) 1–10.
[22] L. Fagiani, N. Granchi, A. Zilli, C. Barri, F. Rusconi, M. Montanari, M. Bollani, Linear and nonlinear optical properties of dewetted SiGe islands, Opt. Mater. X 13 (2022), 100116.